Angewandte Chemie
Eine Zeitschrift der Gesellschaft Deutscher Chemiker

Supporting Information

Coke Formation in a Zeolite Crystal During the Methanol-to-Hydrocarbons Reaction as Studied with Atom Probe Tomography

Joel E. Schmidt, Jonathan D. Poplawsky, Baishakhi Mazumder, Özgün Attila, Donglong Fu, D. A. Matthijs de Winter, Florian Meirer, Simon R. Bare, and Bert M. Weckhuysen**

anie_201606099_sm_miscellaneous_information.pdf

1. Experimental Details

1.1 Sample preparation

The large coffin-shaped ZSM-5 crystals (~ 20×20×100 μm^3) have been provided by ExxonMobil (Machelen, Belgium) and their synthesis has been previously reported.[1] The crystals were calcined at 823 K (ramp rate of 5 K/min, 6 h hold) followed by triple ion exchange with a 10 wt% ammonium nitrate (>99%, Acros Organics) solution at 353 K. Then, the material was converted into proton form by calcination at 823 K (ramp rate of 5 K/min, 6 h hold).

1.2 MTH reaction

MTH reactions were performed in an in-situ reaction cell (THMS 600, Linkam Scientific Instruments) equipped with a temperature controller. Single, large zeolite crystals were placed on a glass plate in the reaction cell and subsequently heated to 393 K (5 K/min for 30 min) under an oxidative atmosphere with an O_2 flow of 20 mL/min. Afterwards, the temperature was increased to 773 K (5 K/min) under the same flow conditions and kept at that temperature for 60 min. Then the temperature was decreased to the reaction temperature of 623 K (350°C) under an inert atmosphere of 20 mL/min N_2 flow. Once the temperature had stabilized, the N_2 flow was changed to run through a room temperature bubbler containing ^{13}C labeled methanol (99 at. %, Sigma Aldrich, vapor pressure of ~100 mmHg). The reaction was run for 90 min, after which time the methanol flow was removed and the reactor was cooled to room temperature under a flow of 20 mL/min N_2. A reaction time of 90 min was carefully chosen to ensure the crystals had sufficient occluded coke for analysis (shown in Figure S1), but were not yet deactivated, demonstrated in our group's previous work using this material.[2] It is important to note that ^{13}C labeled methanol was used, as the previous APT study showed the presence of residual carbon inside the unreacted, calcined material, which was attributed to species absorbed from the air during material handling, contamination during sample preparation or incomplete removal of the template.[3]

1.3 Needle preparation

After reaction, a crystal was prepared for APT analysis using FIB-milling. SEM images of the locations of the lift-outs and needles are given in Figure S2. A single cross section close to the triangular edge of the crystal was selected for APT analysis, such that it would contain 5 out of 6 conjoined hourglass-like prisms forming the MFI crystal. Sample lift-out and needle preparation were done using standard specimen preparation techniques utilizing Si micro-tip arrays purchased from CAMECA.[4] Two lift-outs were prepared from the cross section, one bisecting the cross section and the other from closer to the edge. The location of the lift-outs is shown in Figure S2. A number of needles for APT analysis were then prepared from each lift-out, and their locations are shown in Figure 1 and Figure S2. These locations are important for understanding the results from APT. Although 11 needles were prepared, only 4 data sets were successfully collected, as material fracture and data collection failure (see section 2.1) are common during APT, especially with samples exhibiting low conductivity. Material fracture was observed as these are highly inhomogeneous materials and it was more common in coked samples due to the presence of occluded hydrocarbons. Images of the 4 successful needles before APT analysis can be found in Figure S3.

1.4 APT experimental information

The needle specimens were transferred to the LEAP 4000XR local electrode atom probe equipped with laser pulsing capabilities and an energy compensating reflectron lens located within the Center for Nanophase Materials Sciences (CNMS) at Oak Ridge National Laboratory (ORNL). The specimens were run in laser pulse mode with a laser energy of 200 pJ, base temperature of 40 K, pulse repetition rate of 200 kHz, and a detection rate of 1 atom per 200 pulses. The detector has an efficiency of ~37%.

2. APT Data Analysis

All error analyses were calculated from counting statistics using the method described in reference [5]. In all subsequent discussions, consistent with the terminology used in APT work, 'bulk' refers to the entire needle, 'matrix' refers to the atoms that remain after clusters are removed, and solute refers to the element(s) of interest in cluster analysis. See reference [6] for further details and definitions. In all APT analyses, a small amount of gallium was found to be present due to the FIB-cutting process. All compositional percentages referred to in this work are atomic percentages. For the compositional analysis a background correction was not performed.

2.1 Data analysis for zeolitic materials

The non-conductive nature of the materials used in this study complicates the data collection. The pulsed laser heating helps to overcome these difficulties. Additionally, the presence of coke further complicates the mass spectra. Sample heating creates issues with processing the sample mass spectra as it creates thermal tails in the data. Due to this issue not all collected data sets gave reliable, quantitative results. Additionally, the coked materials were susceptible to fracture under APT conditions, resulting in only 4 complete data sets even though more needle data collections were attempted. Assignments of the peaks in the mass spectra for MTO reacted ZSM-5 crystals was not trivial. It was necessary to analyze an unreacted crystal as a reference and the comparison with this material allowed for correct assignments of peaks corresponding to Al, ^{13}C and Si ionized species.

The Si/Al ratio found in the needles is higher than the bulk ratio of the crystals and there are two main explanations for this observation. The first is that the needles are possibly chosen from areas that have very high Si/Al ratios. Compositional inhomogenities have been reported numerous times for this material. A second reason for this observation is that it is possible that aluminum is susceptible to multiple, simultaneous detector hits, resulting in the loss of counts. This is a known phenomenon for boron (directly above aluminum on the periodic table) and oxides in general.[6] Therefore, it is also possible that this effect is leading to a lower detection of aluminum.

2.2 Isosurface analysis

Isosurface analysis is extensively discussed in reference [6] and the references contained therein. The isosurface analysis is initiated by creating a 3-D grid in concentration space. After this grid is created, 3-D surfaces connecting points of equal elemental concentration can be generated, so called isoconcentration surfaces. These surfaces allow internal features to be identified, and may be defined by a single or multiple elements. The 3-D grid is created by defining a voxel size and delocalization, with the tradeoff that smaller voxels will give a higher resolution but a greater amount of noise. Once the 3-D grids are generated, relevant isosurfaces can be found using concentration thresholds.[6] The importance of the isosurface analysis comes in evaluating the resulting proximity histograms, which allow the border between concentration regions to be evaluated. The exact boundary value chosen is not important as it can change with voxel size and delocalization, what is important is that the proximity histograms allow regions that are poor or rich in specific ion(s) to be identified and separated.

2.3 Cluster analysis

The purpose of cluster analysis is to identify regions where the spacing between solute atoms is smaller than that in the bulk, effectively determining regions that are locally enriched in a specified element, but too small to be observed using the isosurface analysis. For a detailed discussion of the procedure the reader is referred to reference [6]. As a short summary, cluster analysis is initialized by choosing a N_{min} value, which is the minimum number of solute atoms that can form a cluster. With N_{min} set, different values of D_{max} can be evaluated. D_{max} defines the maximum diameter in which another solute atom must be found to form a cluster (one additional solute atom must be found for order =1, higher orders are also possible with more than one solute atom required to fall within D_{max}). A

minimum value of D_{max} is established such that clusters containing at least N_{min} atoms are identified. There are additional parameters that are used in the analysis, and matrix atoms contained in the cluster can also be identified. The key element of cluster analysis is how the parameters are determined and significant clustering is identified. The significance test is accomplished by first taking the number of solute atoms and volume being considered, and randomizing their position using a normal distribution in space. Then, the same cluster analysis is carried out on the randomized data. Once these two data sets are established, the cluster parameters are determined using an iterative process where N_{min} is first set and then the cluster count is plotted as a function of D_{max}. If the solute data is found to be significantly separated from the randomized data (normally chosen as a point where clusters exist in the solute and zero, or a very minimal amount, exist in the randomized data), then D_{max} can be fixed. A fixed D_{max} can then be used to plot cluster count versus cluster size to set an optimal N_{min}. By iterating through these parameters, the optimal cluster D_{max} and N_{min} can be determined, where significant clusters can be found relative to the randomized data.

Another method that is useful in identifying clusters is by directly comparing the nearest neighbor distributions (NNDs) of the solute and randomized data.[7] In doing this, the number of counts is plotted as a function of the atom pair distance. For the randomized data this will, by definition, give a normal distribution. However, if clustering is present, then the solute NNDs will be shifted to a smaller atom pair distance. The NND for the solute data is then described best by at least two Gaussians, one centered at a smaller atom pair distance, representing the clusters, and a second centered at an atom pair distance close to the normal distribution of the randomized data. This makes plotting the NNDs an invaluable tool in cluster analysis.

These deviations from the random distribution can be statistically evaluated using frequency distribution analysis (FDA) and this was applied using CAMECA's IVAS software. The FDA is discussed in references [8–10] and it is used to examine variations in local composition. It is conducted by binning the counts into blocks (block size of 250 was used in this work). Then, the counts can be plotted as a function of local concentration. This distribution is then compared to a random distribution of the data, and a p-test is used to check for statistically relevant clustering (significance level of 0.010 was used).

2.4 Radial Distribution Function

The radial distribution function (RDF) is a powerful tool to examine clustering of small numbers of atoms and test homogeneity and it was applied using CAMECA's IVAS software. The method is extensively discussed in references [11] and [12]. The RDF is conducted by normalizing the local concentration of a selected ion by the bulk concentration, and this is done radially outward from the center of the clusters. In this way it is able to find compositional variations within clusters. Error analyses were conducted using counting statistics; because few ions will be counted near the center of the clusters the error bars are high for the first few data points. The plots presented in Figure S16 report the RDF for the carbon clusters applied to all Al, Si and ^{13}C ions, but only Al and Si are plotted as the normalized ^{13}C values are very high since ^{13}C was the element used to define the clusters.

2.5 APT data analysis workflow

The processing and analysis of the data obtained in an APT experiment is far from trivial and is the subject of active research.[6,8,13,14] Below is a brief outline of the normal workflow used in processing the data. This is not meant to be an exhaustive guide, but rather a brief overview in order to give the reader an idea of the process used.

1. Data collection with an APT instrument.
2. Data processing and reconstruction: When processing zeolite samples it is especially important that all peaks are ranged correctly. The 3-D distribution of all ions can then be generated.
3. Identification of isoconcentration surfaces (isosurfaces): As discussed in section 2.2, isosurface analysis is used to separate large compositional inhomogenities. The isosurfaces are quantified using proximity histograms.

4. Cluster identification: Within subvolumes, isolated using isosurface analysis, both the NNDs and FDAs are used to examine compositional inhomogenities that are not as obvious as isosurfaces. The identification of clusters is an iterative process between comparing the cluster count distribution (CCD) and cluster size distribution (CSD) so that statistically relevant clusters can be identified.
5. Once clusters are determined, the radial distribution function can be used to examine compositional inhomogenities that exist within clusters that may not have been identified using isosurface analysis or cluster analysis.

3. Tables

Table S1. Bulk composition of APT needles 1 to 4. Needle locations are shown in Figures 1 and S2.

Needle	Location	Total matrix atoms	Atomic Composition (%)					
			Al	O	Ga[a]	Si	^{13}C	Si/Al
1	Center	6,114,465	0.22%	62.9%	0.1%	35.6%	1.2%	162.7
2	Center	6,164,300	0.22%	62.7%	0.1%	35.7%	1.2%	152.8
3	Edge	3,580,801	0.36%	61.7%	0.1%	33.6%	4.2%	93.0
4	Edge	1,071,376	0.46%	60.2%	0.7%	32.2%	6.5%	69.0
[a]Gallium is present from the FIB procedure								

Table S2. Frequency Distribution Analysis (FDA) for Al and ^{13}C for needles 1 to 4. FDA is described in section 'APT data analysis' and is conducted by comparing the measured ion distribution with a normalized distribution. The p-test is used to determine whether the measured distribution differs significantly from a normal distribution. From the FDA ^{13}C shows a significant deviation from the random distribution in all needles, while the Al distribution is not significantly different than a random distribution.

Needle	Location	FDA	
		Al p-value	^{13}C p-value
1	Center	0.2804	<0.0001
2	Center	0.2444	<0.0001
3	Edge	0.3311	<0.0001
4	Edge	0.5675	<0.0001
Block size of 250 ions. Significance level of 0.010.			

Table S3. Cluster parameters and compositions for needles 1 to 4.

Needle	Number of Clusters	N_{min}	D_{max} (nm)	Median total ions/cluster	Average total ions/cluster	Range total ions/cluster	Average ^{13}C/cluster	Median ^{13}C/cluster	Range ^{13}C/cluster
1	186	10	0.84	74	95.6	36-1484	15.0	12	10-193
2	152	10	0.81	71	93.5	23-1199	16.0	13	10-144
3	142	16	0.58	91	128.2	42-1414	29.8	21	16-282
4	77	16	0.48	70	98.04	42-580	29.4	23	16-161

	Average Cluster Atomic Composition (%)							
Needle	**Al %**	**O %**	**Ga %[a]**	**Si %**	**^{13}C %**	**Cluster Si/Al**	**Bulk Si/Al**	**Bulk ^{13}C**
1	0.24%	57.18%	0.04%	25.32%	17.23%	102.8	162.7	1.2%
2	0.25%	56.03%	0.07%	24.08%	19.57%	93.8	152.8	1.2%
3	0.26%	55.42%	0.03%	19.80%	24.48%	76.3	93.0	4.2%
4	0.28%	54.83%	0.27%	13.60%	31.01%	48.6	69.0	6.5%

Table S4. Gaussian fits of Nearest Neighbor Distributions (NNDs) for ^{13}C for the NNDs shown in Figures S13 and S14.

Needle	Number of clusters	Randomized NND center (nm)	Observed NND center 1 (nm)	Observed NND center 2 (nm)	Bulk ^{13}C content (%)
1	186	0.949	0.642	0.996	1.23
2	148	0.951	0.633	1.082	1.22
3	142	0.594	0.421	0.635	4.20
4	77	0.527	0.354	0.542	6.55

4. Figures

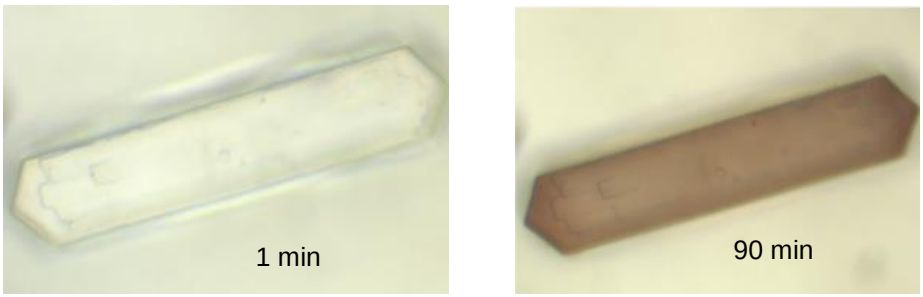

Figure S1. In-situ optical microscope image of a single ZSM-5 crystal during the MTH reaction using ^{13}C labeled methanol after 1 min of reaction (left) and 90 min of reaction (right) at 623 K. In-situ images were acquired during the MTH reaction in the Linkam cell described in Supporting Information section 1.2. The microscope used is an Olympus BX41 and is completely described in reference [2].

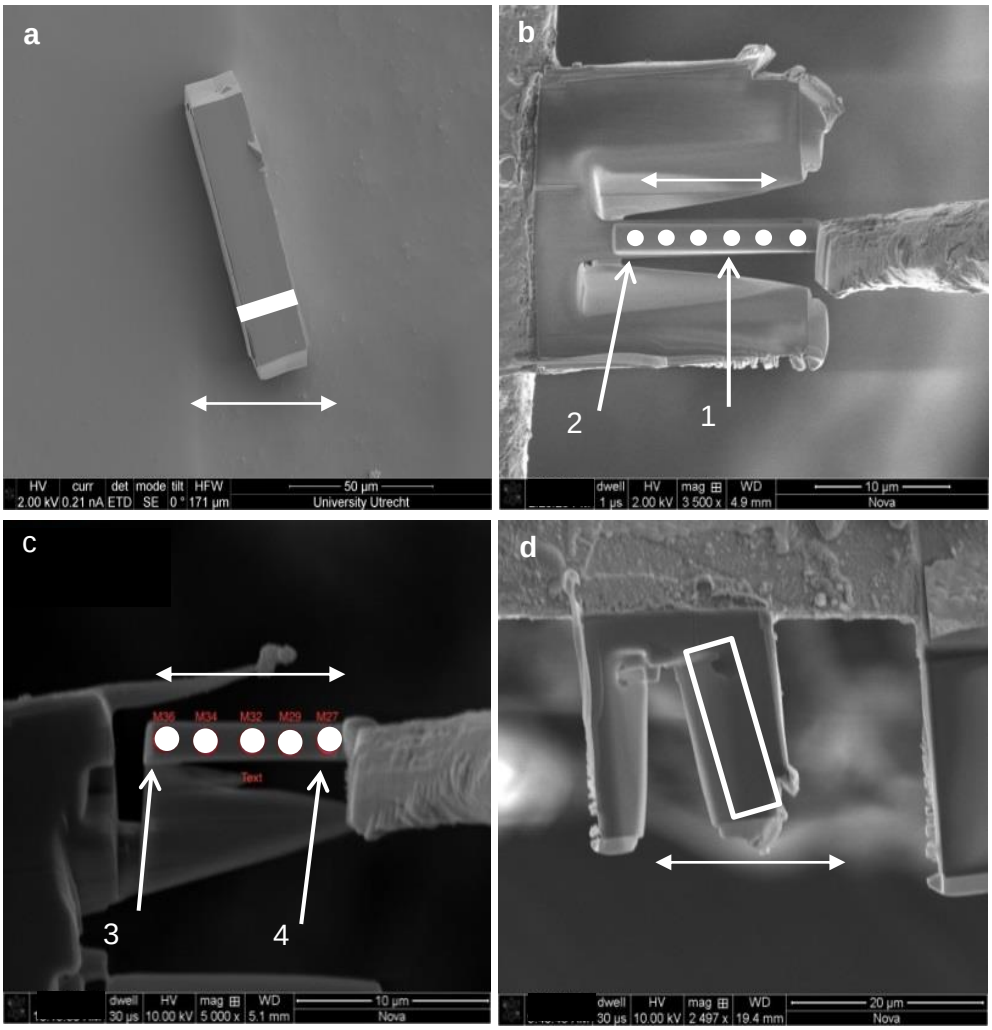

Figure S2. a) Location of the cross section removed from a ZSM-5 crystal after reaction, b) the location of needles 1 and 2 from the section, c) the location of needles 3 and 4, d) the location of liftout 2 where needles 3 and 4 were removed. Scale bars (white double headed arrows) represent 50, 10, 10 and 20 µm for images a to d, respectively.

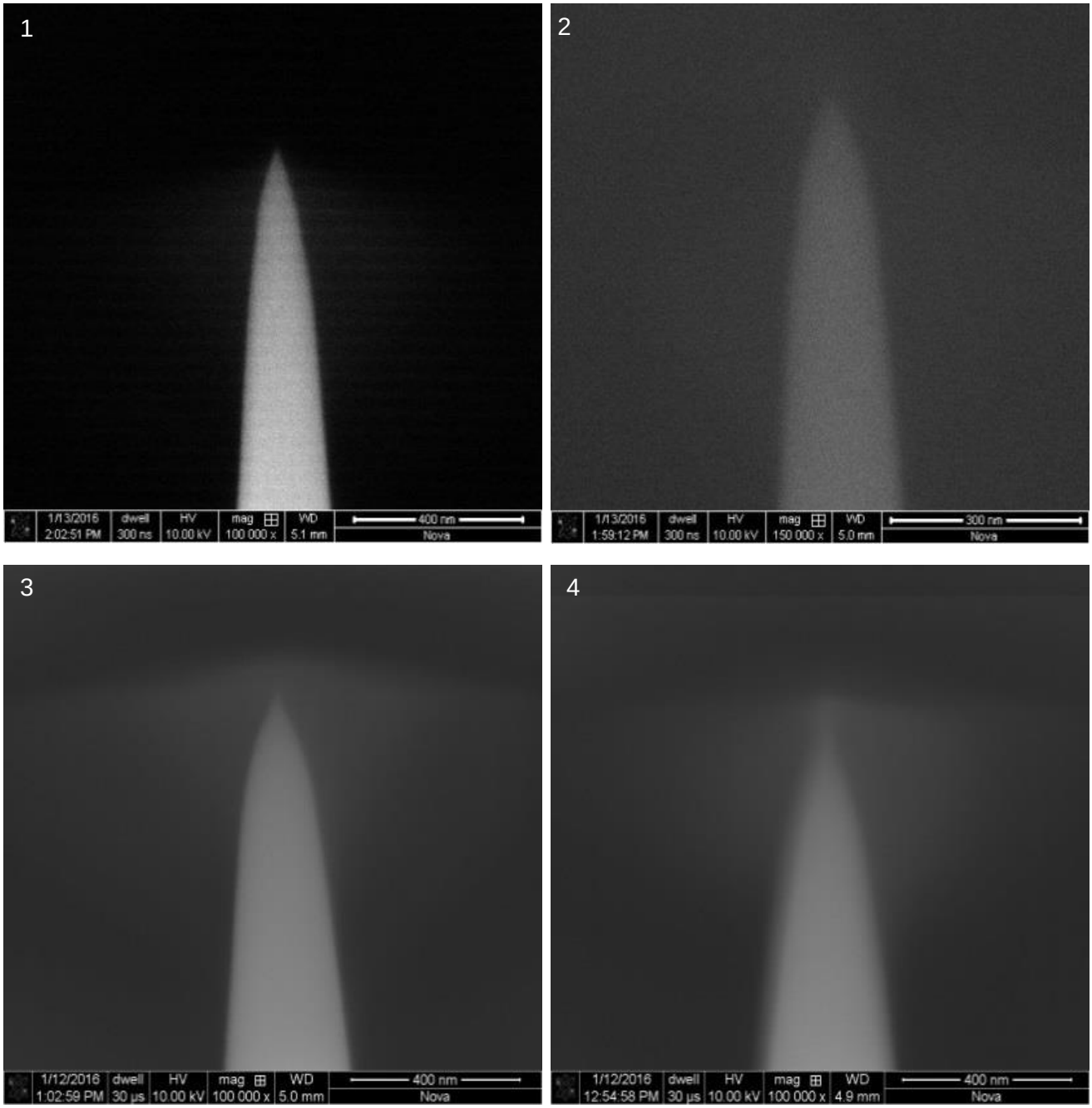

Figure S3. SEM images of needles 1-4 before APT analysis from the positions indicated in Figures 2b and 2c.

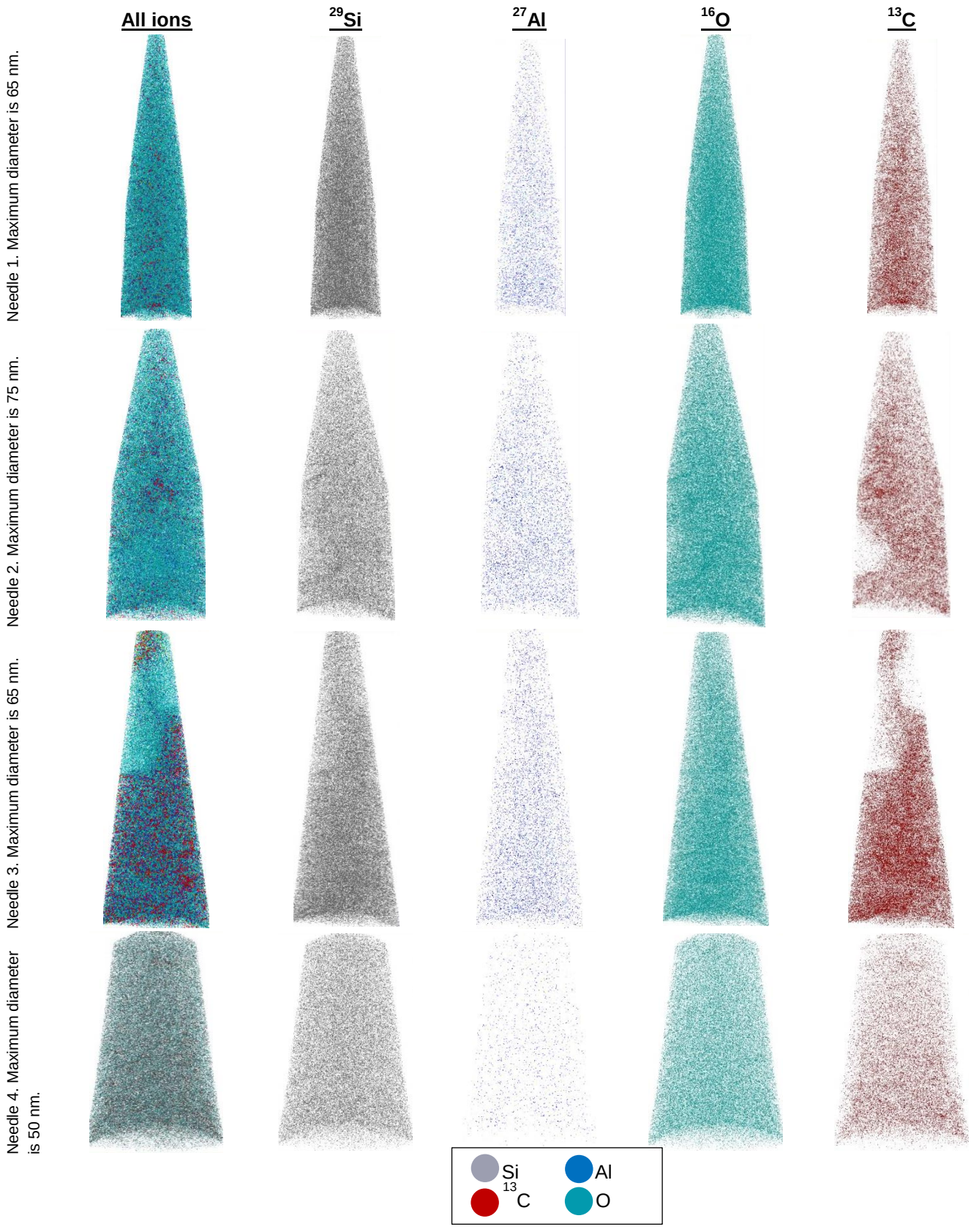

Figure S4. APT 3-D compositional maps of needles 1 to 4. From left to right for each APT needle, the individual needles represent all ions, only Si ions, only Al ions, only O ions and only ^{13}C ions. Additionally, an element color key is below needle 4 with Si in gray, ^{13}C in red, Al in blue and oxygen in green.

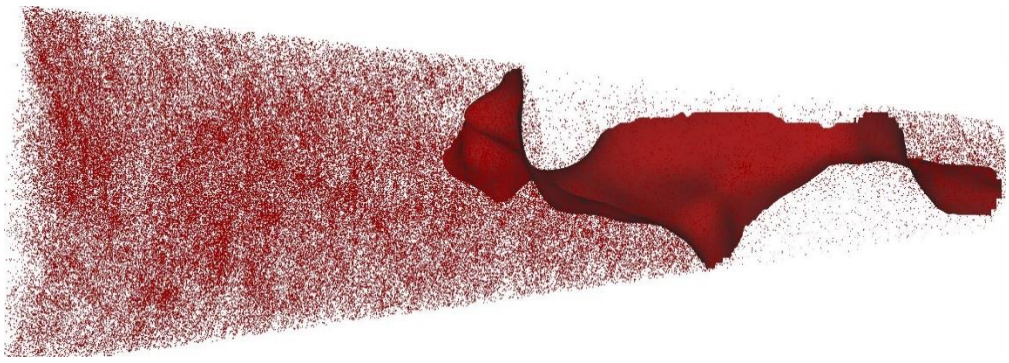

Figure S5. Needle 3 carbon isosurface 1 (3 % ^{13}C boundary). Maximum needle diameter is 65 nm.

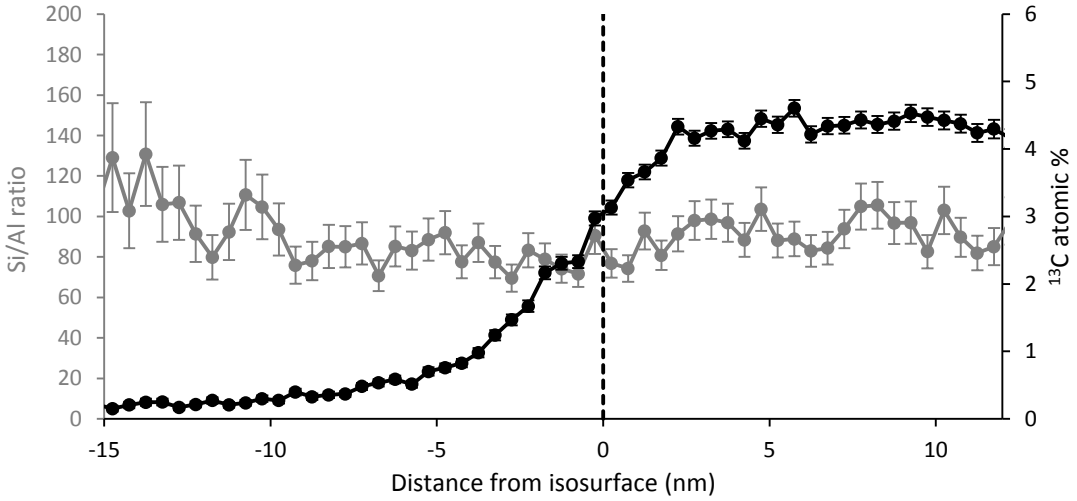

Figure S6. Needle 3 Si/Al ratio and ^{13}C % proximity histogram across the isosurface defined by a 3 % ^{13}C boundary, shown in Figure S5.

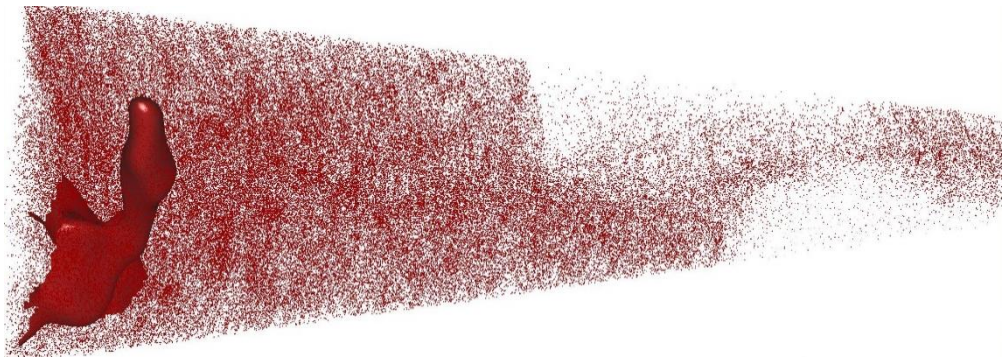

Figure S7. Needle 3 carbon isosurface 2 (3 % ^{13}C boundary). Maximum needle diameter is 65 nm.

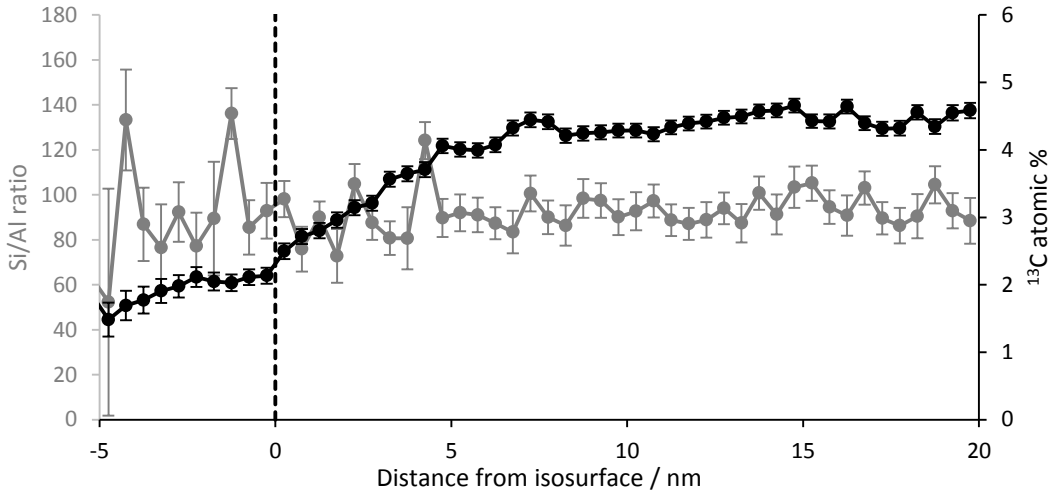

Figure S8. Needle 3 Si/Al ratio and ^{13}C % proximity histogram across isosurface 2 defined by a 3 % ^{13}C boundary, shown in Figure S7.

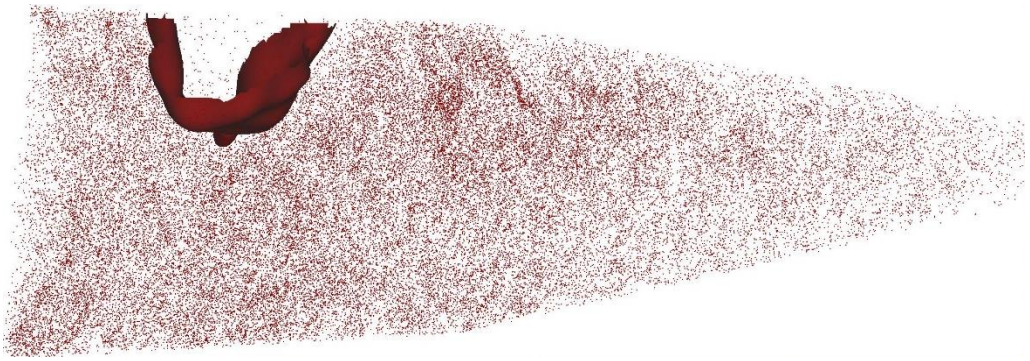

Figure S9. Needle 2 carbon isosurface (0.5 % ^{13}C boundary). Maximum needle diameter is 75 nm. The lower concentration isosurface was defined in needle 2 as the bulk ^{13}C concentration is much lower.

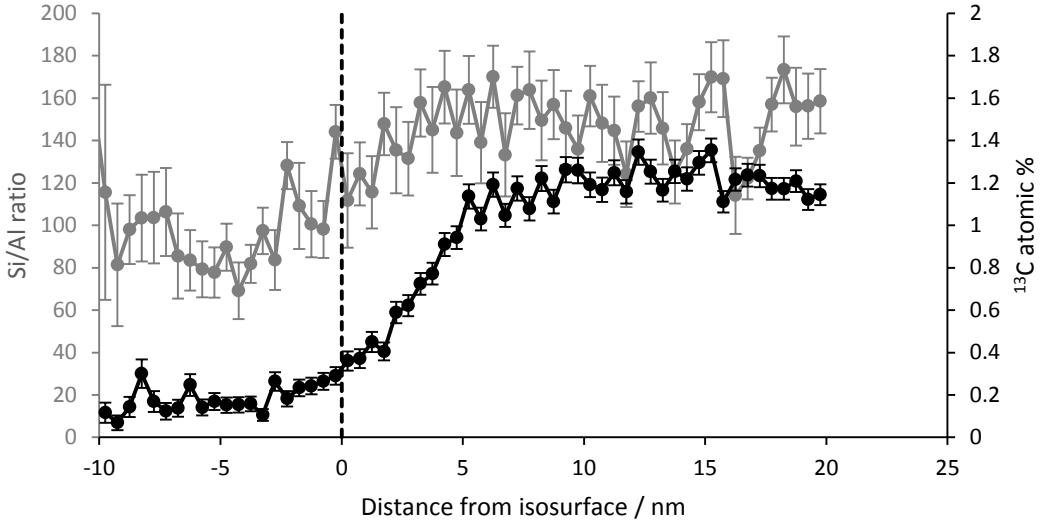

Figure S10. Needle 2 Si/Al ratio and ^{13}C % proximity histogram across the isosurface defined by a 0.5 % ^{13}C boundary, shown in Figure S9.

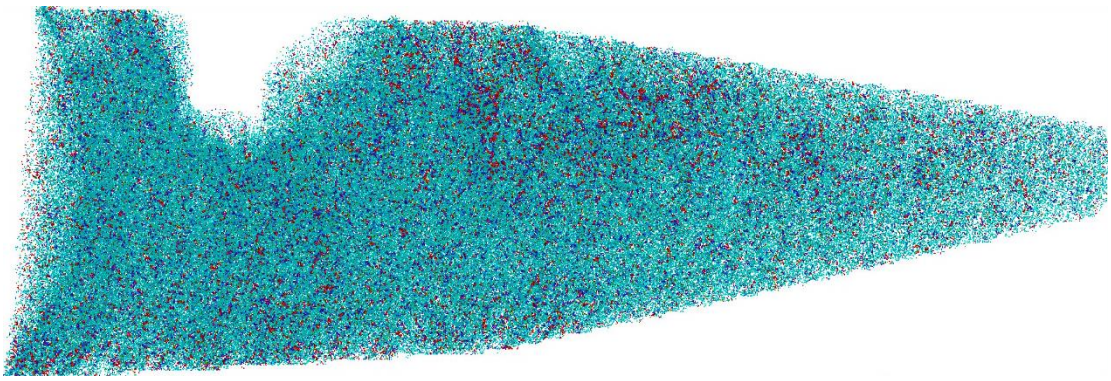

Figure S11. APT 3-D compositional map of needle 2 for all ions after the low carbon region was removed (shown in Figure S9). The remaining region above was used for the cluster analysis, discussed in the main text.

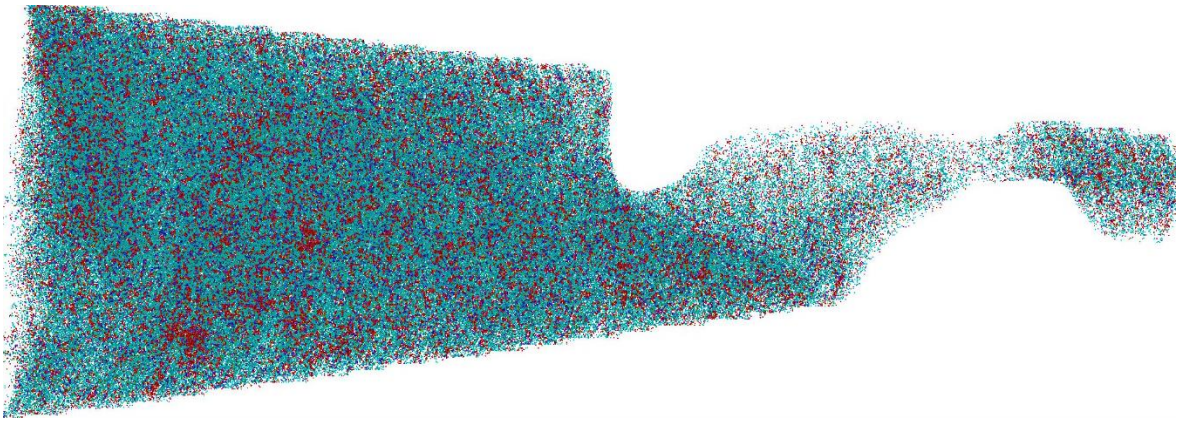

Figure S12. APT 3-D compositional map of needle 3 for all ions after the low carbon region was removed (shown in Figures S5 and S7). The remaining region above was used for the cluster analysis, discussed in the main text.

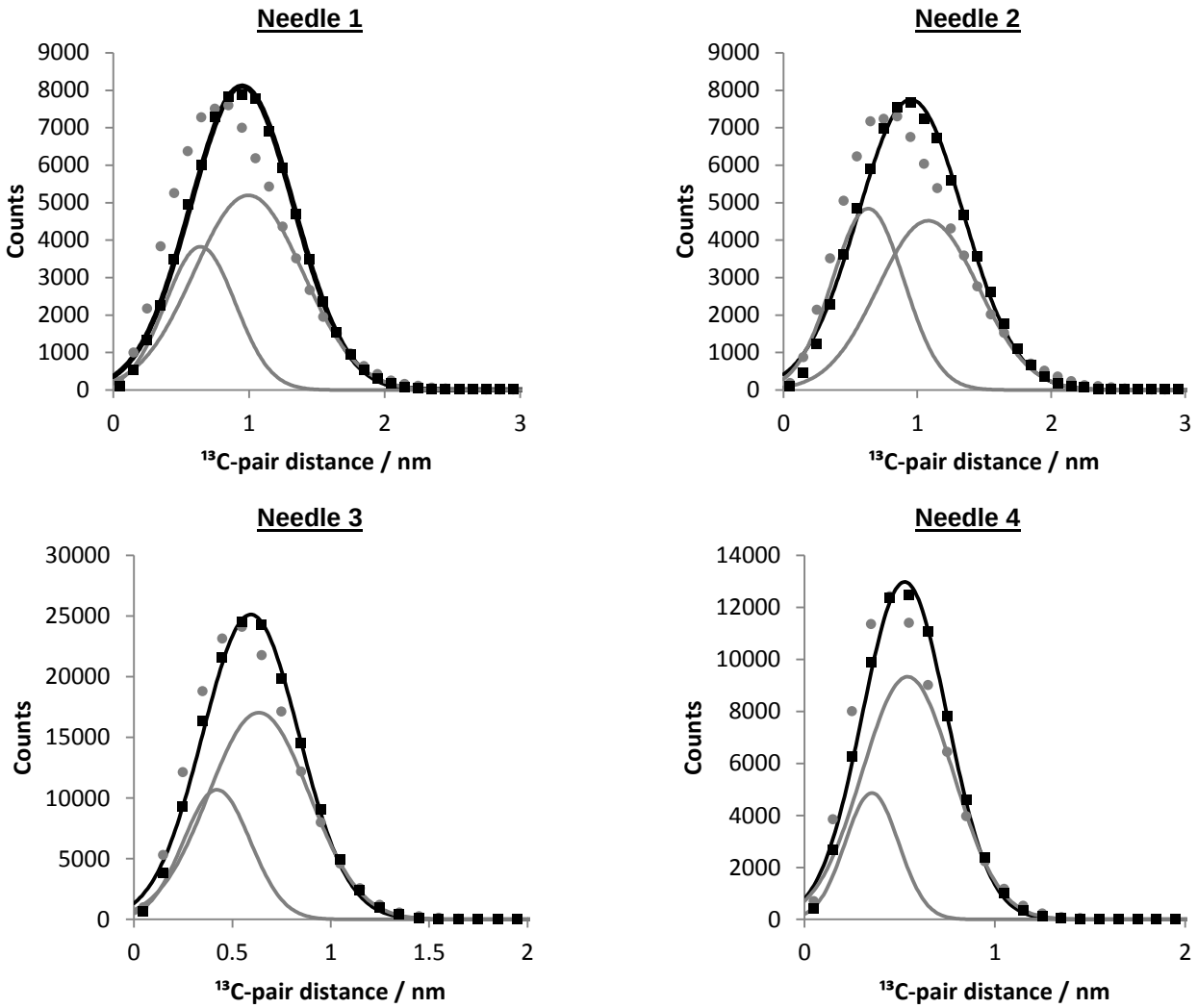

Figure S13. Gaussian fits of the ^{13}C-pair distances (0.1 nm bin size, order = 1). For needles 2 and 3 NNDs were determined only on the carbon rich side of the isosurfaces, such that variations due to these low carbon regions were excluded. Observed data is in gray and randomized data is plotted in black. See the Supporting Information section 2.3 for a more complete explanation of how the NND is conducted.

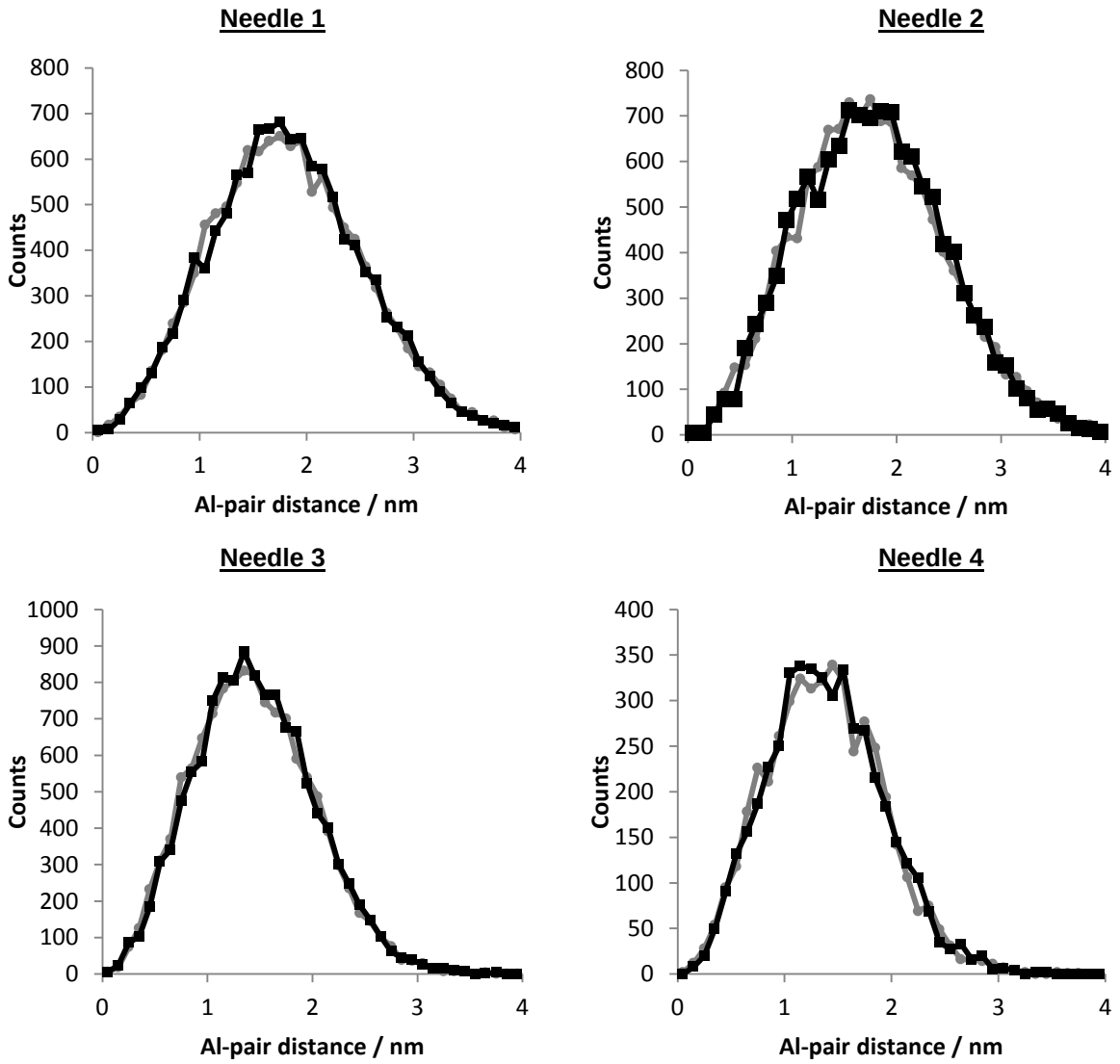

Figure S14. Nearest neighbor distributions (NNDs) for the Al-pair distances (0.1 nm bin size, order = 1). For needles 2 and 3 NNDs were determined only on the carbon rich side of the isosurfaces, such that variations due to these low carbon regions were excluded. Observed data is in gray and randomized data is plotted in black. See the Supporting Information section 2.3 for a more complete explanation of how the NND is conducted.

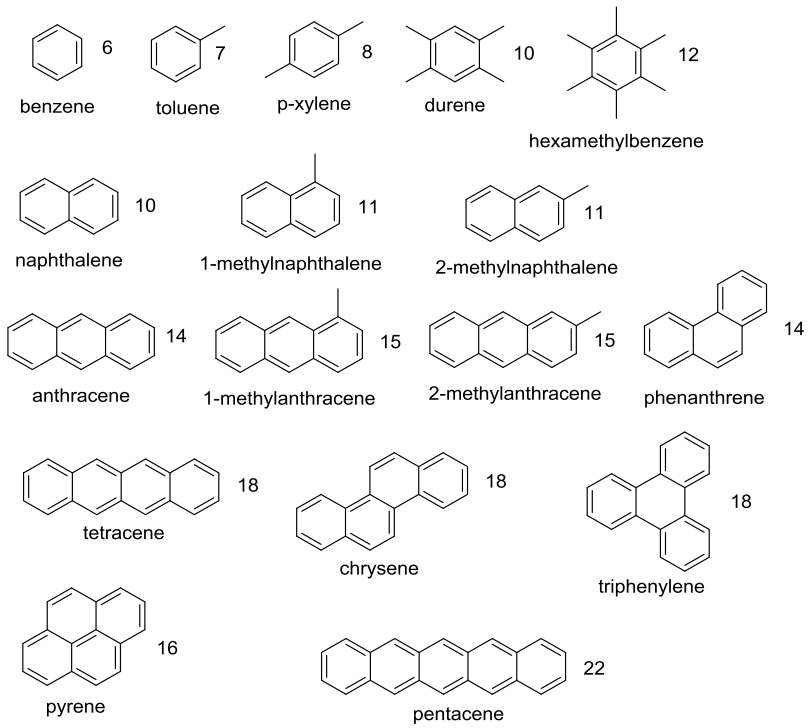

Figure S15. Potential occluded coke species with numbers of carbon atoms per molecule, (poly)methylated versions of the polycyclic species can also exist.[15,16]

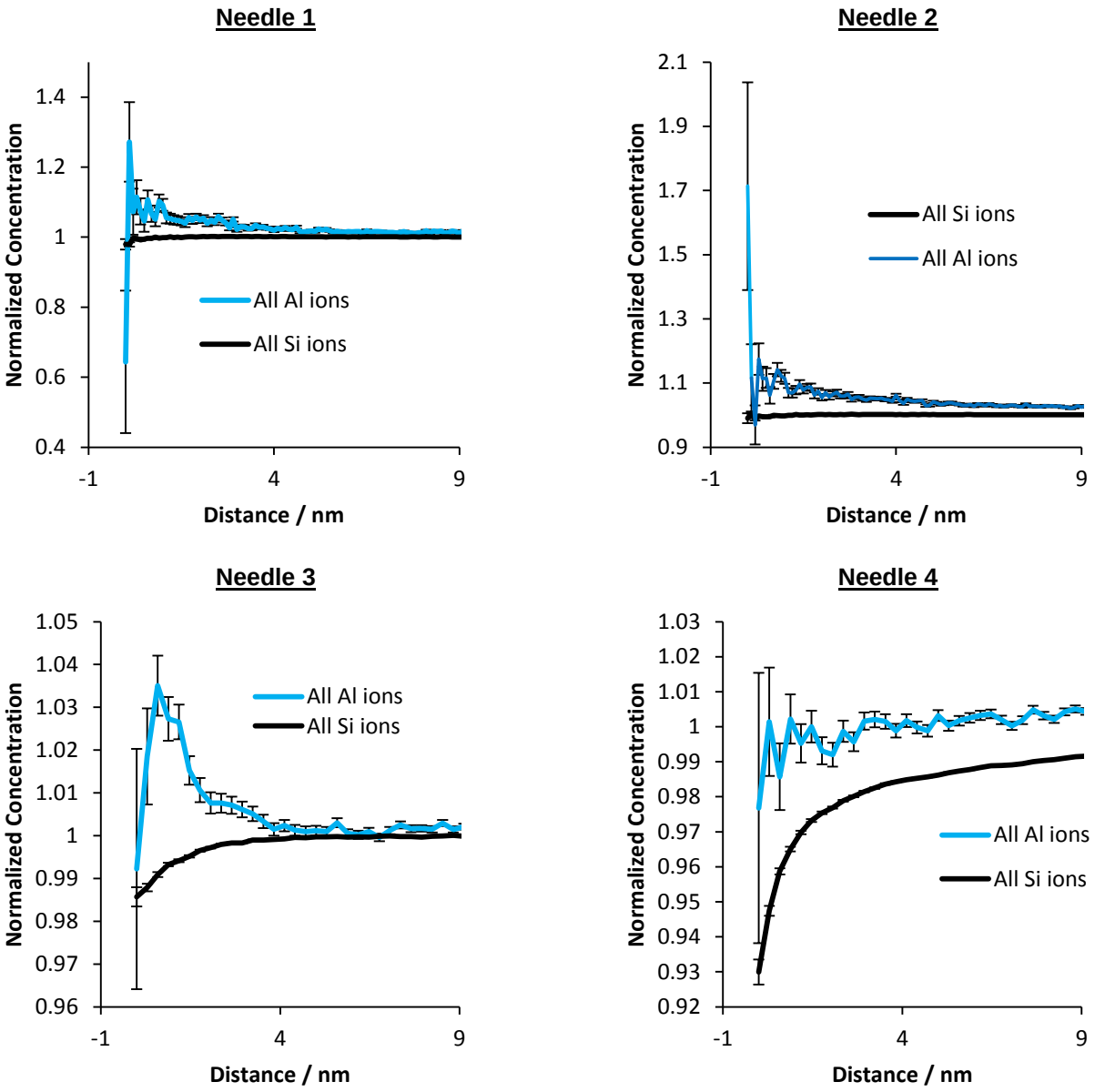

Figure S16. Radial distribution functions for clusters in needles 1 to 4 for all Al and all Si ions. Error bars are determined using counting statistics and at low distances from the centers of the clusters error bars are high due to the low number of ions counted.

5. Supporting Information References

[1] L. R. Aramburo, L. Karwacki, P. Cubillas, S. Asahina, D. A. M. De Winter, M. R. Drury, I. L. C. Buurmans, E. Stavitski, D. Mores, M. Daturi, P. Bazin, P. Dumas, F. Thibault-Starzyk, J. A. Post, M. W. Anderson, O. Terasaki, B. M. Weckhuysen, *Chem. Eur. J.* **2011**, *17*, 13773.

[2] J. P. Hofmann, D. Mores, L. R. Aramburo, S. Teketel, M. Rohnke, J. Janek, U. Olsbye, B. M. Weckhuysen, *Chem. Eur. J.* **2013**, *19*, 8533.

[3] D. E. Perea, I. Arslan, J. Liu, Z. Ristanović, L. Kovarik, B. W. Arey, J. A. Lercher, S. R. Bare, B. M. Weckhuysen, *Nat. Commun.* **2015**, *6*, 7589.

[4] K. Thompson, D. Lawrence, D. J. Larson, J. D. Olson, T. F. Kelly, B. Gorman, *Ultramicroscopy* **2007**, *107*, 131.

[5] M. K. Miller, *Atom Probe Tomography*, Springer US, Boston, MA, **2000**.

[6] D. J. Larson, T. J. Prosa, R. M. Ulfig, B. P. Geiser, T. F. Kelly, *Local Electrode Atom Probe Tomography*, Springer New York, New York, NY, **2013**.

[7] T. Philippe, F. De Geuser, S. Duguay, W. Lefebvre, O. Cojocaru-Mirédin, G. Da Costa, D. Blavette, *Ultramicroscopy* **2009**, *109*, 1304.

[8] M. K. Miller, R. G. Forbes, *Mater. Charact.* **2009**, *60*, 461.

[9] L. T. Stephenson, A. V Ceguerra, T. Li, T. Rojhirunsakool, S. Nag, R. Banerjee, J. M. Cairney, S. P. Ringer, *MethodsX* **2014**, *1*, 12.

[10] M. G. Hetherington, M. K. Miller, *Colloq. Phys.* **1989**, *8*, 535.

[11] C. K. Sudbrack, R. D. Noebe, D. N. Seidman, *Phys. Rev. B* **2006**, *73*, 212101.

[12] D. Haley, T. Petersen, G. Barton, S. P. Ringer, *Philos. Mag.* **2009**, *89*, 925.

[13] T. F. Kelly, M. K. Miller, *Rev. Sci. Instrum.* **2007**, *78*, 031101.

[14] M. K. Miller, T. F. Kelly, K. Rajan, S. P. Ringer, *Mater. Today* **2012**, *15*, 158.

[15] R. Y. Brogaard, B. M. Weckhuysen, J. K. Nørskov, *J. Catal.* **2013**, *300*, 235.

[16] I. Yarulina, J. Goetze, C. Gücüyener, L. van Thiel, A. Dikhtiarenko, J. Ruiz-Martinez, B. M. Weckhuysen, J. Gascon, F. Kapteijn, *Catal. Sci. Technol.* **2016**, *6*, 2663.